INT. J. NUM. METH. HEAT FLUID FLOW, VOL. 3, 517–530 (1993)

AN ARTIFICIAL DISSIPATION SCHEME FOR THE NAVIER–STOKES EQUATIONS

A. KANIEL, M. MOND AND G. BEN-DOR

Pearlstone Center for Aeronautical Engineering Studies, Department of Mechanical Engineering, Ben Gurion University of the Negev, POB 653, Beer Sheva, 84105, Israel

ABSTRACT

Isotropic artificial dissipation is added to the Navier–Stokes equations along with a correction term which cancels the artificial dissipation term in the limit when the mesh size is zero. For a finite mesh size, the correction term replaces the artificial viscosity terms with hyperviscosity terms, i.e., with an artificial dissipation which depends on the fourth derivatives of the velocity. Hyperviscosity more effectively suppresses the higher wave number modes and has a smaller effect on the inertial modes of the flow field than does artificial viscosity. This scheme is implemented using the finite element method and therefore the required amount of dissipation is determined by analysing the discretization on a finite element. The scheme is used to simulate the flow in a driven cavity and over a backward facing step and the results are compared to existing results for these cases.

KEY WORDS Navier–Stokes equations Hyperviscosity Artificial dissipation

INTRODUCTION

Spurious oscillations often occur in numerical solutions of the Navier–Stokes equations which for incompressible flow are:

$$\nabla \cdot \mathbf{V} = 0 \tag{1}$$

$$\frac{\partial \mathbf{V}}{\partial t} + \mathbf{V} \cdot \nabla \mathbf{V} = -\frac{1}{\rho} \nabla P + \nu \nabla^2 \mathbf{V} \tag{2}$$

where $\mathbf{V}$ is the velocity vector, P is the pressure, ρ is the density of the fluid, and ν, which is assumed to be constant, is its kinematic viscosity. In the present work, artificial viscosity terms are added to (2) in order to dampen the spurious oscillations. In addition, in order to decrease the numerical error, a correction term is added so that in the limit when the mesh size is zero it cancels the artificial viscosity terms. This correction term is discussed later. The finite element method is used to implement the above idea.

Determining the amount of artificial viscosity is of crucial importance to the effectiveness of the numerical scheme. This is done by examining the discrete version of (2) on a triangular element with an internal node. The amount of artificial viscosity is now determined by requiring that in the discrete equations, the velocity components at the internal node are some weighted average of the velocity components of its neighbour nodes. This requirement was previously used by Patankar[1] and its implementation here is discussed in detail in later sections.

The present scheme is used to simulate the flow in a driven cavity and over a backward facing step. The numerical results are compared to the numerical results of Ghia *et al.*[2] for a driven

0961–5539/93/060517–14$2.00

Received December 1992
Revised April 1993

cavity and to the experimental and numerical results of Armaly *et al.*[3] for a backward facing step. The present scheme is not limited to a specific type of boundary conditions and it does not require any internal condition, of the type that Thomas *et al.*[4] had to use in their pioneering work on the finite element calculation of convection dominated flows, using a mixed formulation. The present scheme was tailored for the Navier–Stokes equations and therefore simpler test cases such as the solution of the linear convection equation for a scalar variable were not carried out.

THE NUMERICAL SCHEME

Artificial viscosity is presently added to (2) as well as a correction term that eliminates the artificial viscosity where the numerical accuracy is high. The latter depends on Ω which is the vorticity of the flow, i.e. $\Omega = \nabla \times \mathbf{V}$. Thus, instead of (2), a discretization of the following equation is considered:

$$\frac{\partial \mathbf{V}}{\partial t} + \mathbf{V}\cdot\nabla\mathbf{V} = -\frac{1}{\rho}\nabla P + (\nu + \nu_a)\nabla^2\mathbf{V} + \nu_a \nabla \times \Omega \tag{3}$$

where the artificial viscosity ν_a is assumed to be constant, or

$$\frac{\partial \mathbf{V}}{\partial t} + \mathbf{V}\cdot\nabla\mathbf{V} = -\frac{1}{\rho}\nabla P + \nabla[(\nu + \nu_a)\nabla\cdot\mathbf{V}] - \nabla \times [(\nu + \nu_a)\nabla \times \mathbf{V} - \nu_a\Omega] \tag{4}$$

if the artificial viscosity is variable. Note that (4) is identical to (3) when the artificial viscosity is constant, due to the following identity:

$$\nabla^2\mathbf{V} = \nabla[\nabla\cdot\mathbf{V}] - \nabla \times [\nabla\cdot\mathbf{V}] \tag{5}$$

Physically, the second term on the right hand side of (4) is equal to zero because of mass conservation (1). Its discretization will also be equal to zero in the limit of infinite mesh refinement. However, in a finite discretization a computational error of this term exists and it serves to damp out the spurious oscillations. The rotor of Ω is introduced into the second square brackets on the right hand side of (4) in order to make all of the artificial viscosity terms equal to zero in the limit of infinite mesh refinement. However, for this term it is not immediately obvious that its discretization results in a non-zero contribution of the terms multiplied by ν_a. In order to demonstrate that, a finite difference discretization is used for which Ω_{ij} is given by:

$$\Omega_{i,j} = \frac{v_{i+1,j} - v_{i-1,j}}{2\Delta x} - \frac{u_{i,j+1} - u_{i,j-1}}{2\Delta y} \tag{6}$$

where u and v are the velocity components in the directions of the x and y coordinates, respectively, and the corresponding mesh spacings are Δx and Δy. $u_{i,j}$ is the numerical approximation to $u(i\Delta x, j\Delta y)$ and where $v_{i,j}$ and $\Omega_{i,j}$ are similarly defined. The x component of the last term on the right hand side of (4) is therefore given by:

$$-\frac{\partial}{\partial y}[\nabla \times \mathbf{V} - \Omega] \cong \frac{u_{i,j+1} - 2u_{i,j} + u_{i,j-1}}{\Delta y^2} - \frac{u_{i,j+2} - 2u_{i,j} + u_{i,j-2}}{(2\Delta y)^2} = o(\Delta y^2) \tag{7}$$

It is obvious that the sum of the added terms [the artificial dissipation $\nabla \times (\nu_a \nabla \times \mathbf{V})$ plus the correction term $-\nabla x(\nu_a\Omega)$] is not zero but it is small whenever the flow is smooth with respect to the mesh size. A Taylor series analysis of (7) will reveal that the addition of the correction term turned the artificial terms from artificial viscosity terms to hyperviscosity terms, i.e. to an artificial dissipation which depends on the fourth derivative of u. This is done without burdening the programmer with additional boundary conditions. The present work seeks to suppress the

spurious oscillations which often are of the highest wave number resolvable on the computational grid. Hyperviscosity is more suitable for this purpose than artificial viscosity for it more effectively suppresses the higher wave number modes and has a smaller effect on the inertial modes of the flow field.

The use of the auxiliary variable Ω as a computational device, is an innovation of Jiang *et al.*[5,6] who introduced it in the context of their least squares finite element method. In their method, as in the Lax Wendroff/Taylor Galerkin method, the discrete equations are endowed with a significant amount of numerical dissipation although a physically wrong term is not added to the equations. The present scheme reaches the same end with much simpler discrete equations. In addition, the amount of numerical dissipation in the present scheme is not dependent on the size of the time step as it is in both of the other methods. The present scheme is applicable to viscous flows, unlike the Lax Wendroff/Taylor Galerkin method which is limited to hyperbolic equations.

To summarize, instead of directly solving the Navier–Stokes equations, standard Galerkin integrations are performed on the following four equations:

$$u_{,x} + v_{,y} = 0 \tag{8}$$

$$v_{,x} - u_{,y} = \Omega \tag{9}$$

$$\frac{u - u^0}{\Delta t} + (uu)_{,x} + (uv)_{,y} = -\frac{1}{\rho} P_{,x} + [(\nu + \nu_a)(u_{,x} + v_{,y})]_{,x} + [(\nu + \nu_a)(u_{,y} - v_{,x}) + \nu_a \Omega)]_{,y} \tag{10}$$

$$\frac{v - v^0}{\Delta t} + (uv)_{,x} + (vv)_{,y} = -\frac{1}{\rho} P_{,y} + [(\nu + \nu_a)(u_{,x} + v_{,y})]_{,y} - [(\nu + \nu_a)(u_{,y} - v_{,x}) + \nu_a \Omega)]_{,x} \tag{11}$$

where to make the discretization conservative, $V\nabla \cdot V$ was added to the momentum conservation equation whose components are (10) and (11). For completeness, an implicit temporal discretization was introduced in these equations although it is used in this work only when a temporal relaxation is required. Here Δt is the time step and the superscript 0 marks the value of the variable at the previous time step. Note that this formulation is not the standard velocity–vorticity formulation. Therefore this formulation does not lead to the constraints on the integration procedure which are associated with the latter.

Any application of the present scheme requires a method for determining the value of ν_a and the next two sections present such a method for the present finite elements.

ARTIFICIAL DISSIPATION FOR A MODEL EQUATION

Following Patankar[1], a criterion for the amount of artificial dissipation required for a model equation (the constant coefficient convection diffusion equation) is introduced in this section. Subsequently the criterion is corrected to suit the Navier–Stokes equations with a correction term. The model equation is:

$$u \frac{\partial T}{\partial x} + v \frac{\partial T}{\partial y} - \alpha \nabla^2 T = 0 \tag{12}$$

where u and v are the velocity components in the directions of the x and y coordinates, respectively, and α is the thermal diffusivity of the fluid, all of which are constant, and T is the temperature.

To determine the required amount of artificial dissipation the discrete version of this model equation is examined. Therefore the discretization used in this work is introduced. Consider the triangular element shown in *Figure 1*. A function $f(x, y)$ may be approximated by a linear interpolation over such an element, as in:

$$f(x, y) = w_0(x, y) f_0 + w_1(x, y) f_1 + w_2(x, y) f_2 \tag{13}$$

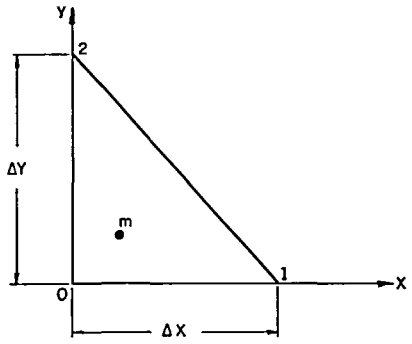

Figure 1 An example element

where f_i is the value of f at the ith vertex and w_i is the distance of the point (x, y) from the side which is opposite the ith vertex, divided by the distance of the ith vertex from the same side. In the right triangle of *Figure 1*, w_1 is $x/\Delta x$, w_2 is $y/\Delta y$ and w_0 is $1 - x/\Delta x - y/\Delta y$ in accordance to the following general rule:

$$w_0 + w_1 + w_2 = 1 \tag{14}$$

This rule may also be used to calculate w_0 for any triangle where w_1 and w_2 are given by:

$$w_1(x, y) = \frac{(x - x_0)(y_2 - y_0) - (x_2 - x_0)(y - y_0)}{2A} \tag{15}$$

$$w_2(x, y) = \frac{(x_1 - x_0)(y - y_0) - (x - x_0)(y_1 - y_0)}{2A} \tag{16}$$

where x_i and y_i are the coordinates of the ith vertex and A is the area of the triangle, i.e. $2A = (x_1 - x_0)(y_2 - y_0) - (x_2 - x_0)(y_1 - y_0)$, and it is assumed that the nodes are numbered in the counterclockwise direction.

A higher order interpolation is achieved by the following approximation for a given function $g(x, y)$:

$$g(x, y) = w_0 g_0 + w_1 g_1 + w_2 g_2 + 27 w_0 w_1 w_2 \left(g_m - \frac{g_0 + g_1 + g_2}{3} \right) \tag{17}$$

where g_0, g_1 and g_2 are the values of g at the vertices and g_m is the value of g at the centroid of the element (i.e. where $x = (x_0 + x_1 + x_2)/3$, $y = (y_0 + y_1 + y_2)/3$ and therefore $w_0 = w_1 = w_2 = 1/3$). This interpolation is linear on the boundaries of the element where $w_0 w_1 w_2$ vanishes and thus ensures the continuity of the interpolation at common boundaries of different elements.

A criterion for the amount of artificial dissipation required for the model equation (12) is now obtained for the case where $T(x, y)$ is approximated by (17). To obtain this criterion, the temperature at the internal node of the element is considered. To determine this temperature, a weighted integration of (18) is performed over the relevant element. The weighting function is $w_0 w_1 w_2$ and the resulting equation is:

$$\left[u \frac{\partial T}{\partial x} + v \frac{\partial T}{\partial y} - (\alpha + \alpha_a) \nabla^2 T \right]_{x = x_m, y = y_m} = 0 \tag{18}$$

where the derivatives of T are obtained by differentiating (17), α_a is the artificial dissipation coefficient which is added to the equation and which is the subject of this discussion. For the

element of *Figure 1*, (18) is:

$$u\frac{T_1 - T_0}{\Delta x} + v\frac{T_2 - T_0}{\Delta y} + 9(\alpha + \alpha_a)\left(\frac{2}{\Delta x^2} + \frac{2}{\Delta y^2}\right)\left(T_m - \frac{T_0 + T_1 + T_2}{3}\right) = 0 \tag{19}$$

and from this last equation we calculate that:

$$T_m = \frac{T_0 + T_1 + T_2}{3} - \frac{u\dfrac{T_1 - T_0}{\Delta x} + v\dfrac{T_2 - T_0}{\Delta y}}{9(\alpha + \alpha_a)\left(\dfrac{2}{\Delta x^2} + \dfrac{2}{\Delta y^2}\right)} \tag{20}$$

It is readily seen that in the absence of convection T_m is the arithmetic average of the temperatures of the surrounding vertices. However, if the convection is significant, T_m may actually be larger than all of the surrounding temperatures. This unphysical behaviour is obviously a computational error and it is the source of the spurious oscillations whose prevention is sought. To reach this goal the artificial dissipation coefficient is increased to ensure that the coefficients of all of the temperatures on the right hand side of (20) are not negative. This is an extension to a finite element discretization of the basic approach of Patankar[1]. Accordingly, the following requirement is imposed:

$$\frac{1}{3} - \frac{\max\left(\dfrac{u}{\Delta x}, \dfrac{v}{\Delta y}, -\dfrac{u}{\Delta x}, -\dfrac{v}{\Delta y}\right)}{9(\alpha + \alpha_a)\left(\dfrac{2}{\Delta x^2} + \dfrac{2}{\Delta y^2}\right)} \geqslant 0 \tag{21}$$

In order to fulfill this requirement α_a is given by:

$$\frac{\alpha_a}{\alpha} = \max\left(0, \frac{u/\Delta x}{3\alpha\left(\dfrac{2}{\Delta x^2} + \dfrac{2}{\Delta y^2}\right)} - 1, \frac{v/\Delta y}{3\alpha\left(\dfrac{2}{\Delta x^2} + \dfrac{2}{\Delta y^2}\right)} - 1, \frac{-u/\Delta x - v/\Delta y}{3\alpha\left(\dfrac{2}{\Delta x^2} + \dfrac{2}{\Delta y^2}\right)} - 1\right) \tag{22}$$

This choice of α_a ensures that T_m is a weighted average of the three neighbouring temperatures, as it should be, and thus prevents T_m from exceeding their extremum value. This choice of α_a also ensures that if the system of equations is diagonally dominant, (19) will not disrupt the diagonal dominance. Note that α_a is about a sixth of the classic $Vh/2$ if $h = \Delta x = \Delta y$.

Especially important is the special dependence of α_a on the aspect ratio of the element. This special dependence on the elemental geometry, rather than an intuitive derivation of an expression for h, is one of the two main contributions of the present work. Without regard to the flow direction, it eliminates the artificial dissipation where either Δx or Δy is very small so if the molecular dissipation is sufficient, it is not artificially increased. This is a truly two-dimensional criterion for the required amount of dissipation, unlike the one-dimensional TVD criterion, or the results of the various Riemann solvers or even Patankar's[1] criterion which assigns to each direction an artificial dissipation coefficient which depends only on the grid spacing in that direction.

If the element is not a right triangle, the following expressions are substituted into (18):

$$\left.\frac{\partial T}{\partial x}\right|_{x=x_m, y=y_m} = \frac{(T_1 - T_0)(y_2 - y_0) - (T_2 - T_0)(y_1 - y_0)}{2A} \tag{23}$$

$$\left.\frac{\partial T}{\partial y}\right|_{x=x_m, y=y_m} = \frac{(x_1 - x_0)(T_2 - T_0) - (x_2 - x_0)(T_1 - T_0)}{2A} \tag{24}$$

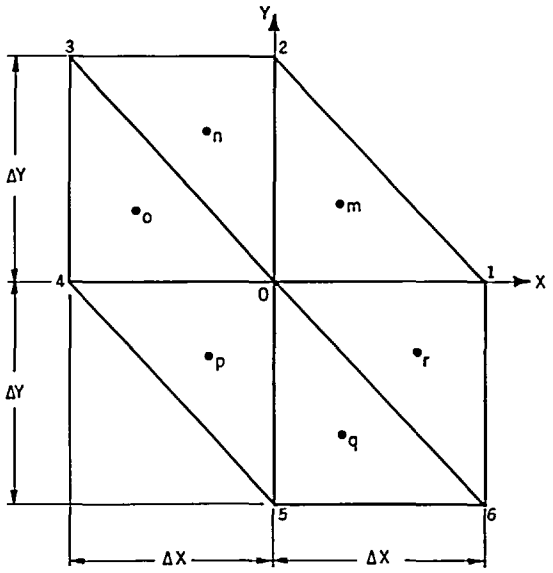

Figure 2 A structured grid segment

$$\nabla^2 T|_{x=x_m, y=y_m} = -9B^2\left(T_m - \frac{T_0 + T_1 + T_2}{3}\right) \tag{25}$$

where $B^2 = \sum l_i^2/(2A)^2$ and l_i is the length of the ith side of the triangular element. As was previously explained, when the above expressions are substituted into (18), α_a is determined such that the coefficients of T_0, T_1 and T_2 are all of the same sign. The result is:

$$\frac{\alpha_a}{\alpha} = P_e \tag{26}$$

where P_e is an elemental Peclet number which is given by:

$$P_e = \max_i\left(0, \frac{u(y_i - y_{i^*}) + v(x_{i^*} - x_i)}{6\alpha AB^2} - 1\right) \tag{27}$$

where i^* is the vertex next to i in the counterclockwise direction.

Equations (26) and (27) are the proposed criterion for the required amount of isotropic artificial dissipation for an element of a general orientation and geometry. The equations were derived by analysing the discretization which relates to the internal nodes. Therefore for completeness, this section concludes with a discussion of the discretization which relates to a vertex node. Such is the equation that results from the weighted integration of (12) over the structured grid segment which is shown in *Figure 2*:

$$\frac{u}{6}\left\{4\frac{T_1 - T_4}{2\Delta x} + \frac{T_2 - T_3}{\Delta x} + \frac{T_6 - T_5}{\Delta x}\right\} + \frac{9u}{40}\frac{dT_m + dT_r - dT_0 - dT_p}{\Delta x}$$
$$+ \frac{v}{6}\left\{4\frac{T_2 - T_5}{2\Delta y} + \frac{T_3 - T_4}{\Delta y} + \frac{T_1 - T_6}{\Delta y}\right\} + \frac{9v}{40}\frac{dT_m + dT_n - dT_p - dT_q}{\Delta y}$$
$$- (\alpha + \alpha_{a0})\left[\frac{T_1 - 2T_0 + T_4}{\Delta x^2} + \frac{T_2 - 2T_0 + T_5}{\Delta y^2}\right] = 0 \tag{28}$$

where α_{a0} is given by $\int w_0 \alpha_a \nabla^2 T \, dA / \int w_0 \nabla^2 T \, dA$. The terms with the letter subscripts in (28) are the contribution of the internal nodes to the equation, and they are defined by expressions such as:

$$dT_m \equiv \left(T_m - \frac{T_0 + T_1 + T_2}{3} \right) \tag{29}$$

In (28), the nodal temperatures T_3 and T_6 do not appear in the dissipation terms and therefore increasing the artificial dissipation α_a coefficient cannot make their coefficients negative, and therefore T_0 cannot be made the average of all of the variables which appear in (28). Nevertheless, the equation is not prone to producing spurious oscillations. To show that, dT_m and similar expressions are replaced using (18), (25) and (29). The result is:

$$\frac{u}{6}\left\{4\frac{T_1 - T_4}{2\Delta x} + \frac{T_2 - T_3}{\Delta x} + \frac{T_6 - T_5}{\Delta x}\right\} - \frac{u}{40}\frac{\left[\frac{\mathbf{V}\cdot\nabla T}{\alpha + \alpha_a}\right]_m + \left[\frac{\mathbf{V}\cdot\nabla T}{\alpha + \alpha_a}\right]_r - \left[\frac{\mathbf{V}\cdot\nabla T}{\alpha + \alpha_a}\right]_0 - \left[\frac{\mathbf{V}\cdot\nabla T}{\alpha + \alpha_a}\right]_p}{B^2 \Delta x}$$

$$+ \frac{v}{6}\left\{4\frac{T_2 - T_5}{2\Delta y} + \frac{T_3 - T_4}{\Delta y} + \frac{T_1 - T_6}{\Delta y}\right\} - \frac{v}{40}\frac{\left[\frac{\mathbf{V}\cdot\nabla T}{\alpha + \alpha_a}\right]_m + \left[\frac{\mathbf{V}\cdot\nabla T}{\alpha + \alpha_a}\right]_n - \left[\frac{\mathbf{V}\cdot\nabla T}{\alpha + \alpha_a}\right]_p - \left[\frac{\mathbf{V}\cdot\nabla T}{\alpha + \alpha_a}\right]_q}{B^2 \Delta y}$$

$$- (\alpha + \alpha_{a0})\left[\frac{T_1 - 2T_0 + T_4}{\Delta x^2} + \frac{T_2 - 2T_0 + T_5}{\Delta y^2}\right] = 0 \tag{30}$$

where a letter subscript of a term in square brackets indicates that this term is evaluated at the appropriate node. Equation (30) is clearly endowed with two kinds of dissipative terms. An isotropic dissipation term which is a discretization of $(\alpha + \alpha_{a0})\nabla^2 T$ and a stream-wise upwinding term which is a discretization of $\mathbf{V}\cdot\nabla\left[\frac{\mathbf{V}\cdot\nabla T}{\alpha + \alpha_a}\right] \Big/ (40B^2)$. The latter is the only difference between (30) and the discretization by linear elements of the same model equation.

ARTIFICIAL VISCOSITY COEFFICIENT

We now turn back from the model equation to equations (8)–(11) and search for the artificial viscosity coefficient for (10) and (11). Equations (8)–(11) are discretized using a linear interpolation for the vorticity and the pressure and to satisfy the Babuska–Brezzi condition the interpolation of (17) is used for the velocity components. This admissibility criterion ensures that the number of unknown nodal velocity components is larger than the number of discrete mass conservation equations. The interpolations are also C^0 continuous and therefore suitable for use in the solution of second order equations. The artificial dissipation coefficient was derived by considering the discretization for the convection and diffusion terms, based on the interpolation of (17). However, it did not account for the pressure and the vorticity terms which appear in (8)–(11). In addition, the coefficients u, v and α_a were held constant over each element in the derivation. Therefore the results of (26) and (27) are the starting point of the present empirical search for the artificial viscosity coefficient for (10) and (11).

In the present section four different artificial viscosity coefficients are presented in the order of increasing accuracy. The first one of these four coefficients is:

$$\frac{v_a}{v} = P_e \tag{31}$$

where P_e is defined by (27), but v rather than α are used in its calculation. P_e is a function of u

and v which are variables. Therefore v_a is calculated at each integration point, using the local values of u and v.

The second artificial viscosity coefficient is:

$$\frac{v_a}{v} = \left|1 - \frac{v_{,x} - u_{,y}}{\Omega}\right|^d P_e \tag{32}$$

In this case, in regions where Ω varies slowly, the artificial dissipation coefficient is greatly reduced. The exponent d is an empirical constant that depends on the order of the interpolations and for the present case the value of 0.2 was used because with higher values the convergence properties of the scheme deteriorated.

The third artificial viscosity coefficient which is examined is a function of P_e which for high values of P_e approaches (31) while at low values of P_e it approaches zero much faster than the right hand side of (31):

$$\frac{v_a}{v} = \frac{P_e^2}{P_e + f} \tag{33}$$

This formulation was chosen because it ensures that both v_a and its derivatives with respect to the velocity components are continuous functions of the velocities. This is a very helpful feature when a Newton–Raphson scheme is used to solve the discrete equations; f is an empirical constant and the value of 10 was used because with higher values the convergence properties of the scheme deteriorated.

The fourth artificial viscosity coefficient is a combination of the last two:

$$\frac{v_a}{v} = \frac{P_e^2}{P_e + f}\left|1 - \frac{v_{,x} - u_{,y}}{\Omega}\right|^d \tag{34}$$

Equation (34) decreases the value of v_a below the value given by (31) both where Ω varies slowly, and where P_e/f is small. The next section shows that this equation yields more accurate results than the previous formulations.

NUMERICAL RESULTS DERIVED USING A COARSE GRID

The artificial viscosity coefficients of the last section were employed in the simulation of the flow over a backward facing step—a realistic internal flow situation which is endowed with a variety of boundary conditions and a complicated flow behaviour. The present results compare favourably with the experimental results of Armaly *et al.*[3] and are by far more accurate then the numerical results which Armaly *et al.*[3] calculated using TEACH, a commercial finite difference code.

The experimental results of Armaly *et al.*[3] are two-dimensional up to a Reynolds number of 400. Their numerical results and the present ones are therefore applicable only in this range. To choose one out of the four artificial dissipation coefficients of the previous section, these coefficients are used to reproduce the flow field in this range on a coarse grid. Even beyond a Reynolds number of 400 and although a very coarse grid is used the present scheme produces physically reasonable results. This is true for all of the four artificial viscosity coefficients given by (31)–(34) and it is also true if the vertex nodes of the grid are reconnected in a different way. The results for a finer grid are presented in the next section.

Figure 3 is a vector plot of the backward facing step problem and in it we define the re-attachment length x_1 and the step size S. A portion of the present grid is shown in the upper part of the Figure. The step size S is 49/101 of the full channel width and the calculations were carried over a domain which extends from 3 full channel widths upstream of the expansion (about 6 local channel widths) to 21 channel widths downstream of the expansion. In the inflow

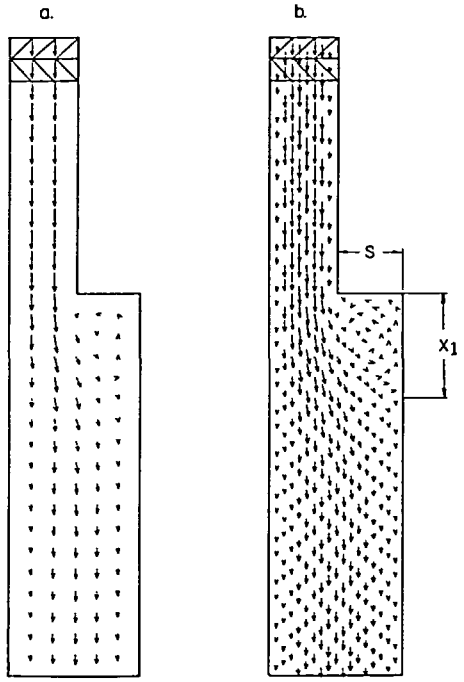

Figure 3 The backward facing step: (a) vectors emanating from the elements vertices; (b) vectors emanating from all of the nodes

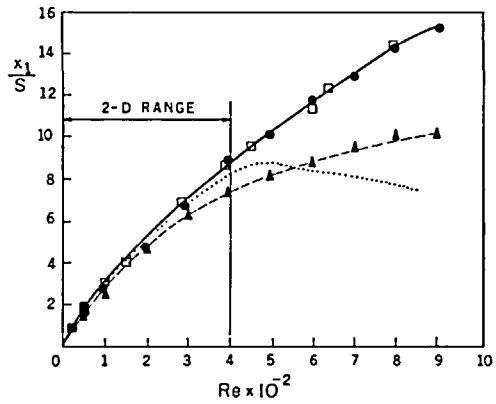

Figure 4 The re-attachment length: □, experimental results of Armaly *et al.*[3] for the centreline of the experimental setup; ·····, numerical results of Armaly *et al.*[3]; –●–, –▲–, present results derived using (34) and (31) respectively

boundary, a zero tangential velocity was specified and a parabolic normal velocity distribution was prescribed. This is in agreement with the experimental observations of Armaly *et al.*[3]. At the outflow boundary, the normal derivative of the tangential velocity is set to zero. A zero value was also specified for the divergence of the velocity on the boundary. The pressure was specified at the corner node shared by the outflow boundary and the wall on the right side. Numerical experiments were conducted and showed that the type of the outflow conditions can be changed without any significant effect on the results.

Figure 4 compares the present results for the re-attachment length with the experimental and numerical results of Armaly *et al.*[3]. The squares mark the experimental results of Armaly *et al.*[3] and a dotted line marks their numerical results. The triangles and the circles represent the present results as obtained using the artificial viscosity coefficients given by (31) and (34), respectively. *Figure 4* clearly shows that results obtained using (34) are by far superior to the results obtained using (31). The results derived using the artificial viscosity coefficients given by (32) and (33) are not shown for aesthetic reasons. They are quite similar to each other and are in the middle between the shown results. Hence, the accuracy of the results clearly increases when less artificial viscosity is used on this coarse grid, even below the relatively little artificial viscosity given by (31). This indicates the importance of accurate criteria for marginal artificial dissipation.

Below a Reynolds number of about 200 it is possible to have results without artificial viscosity and these are identical to the results which are shown. This validates the expectation that the scheme will produce accurate results wherever the grid is fine in relation to the flow properties (wherever the mesh spacing is small in relation to v/V).

Besides the points which are shown in *Figure 4*, a few points were calculated with a similar

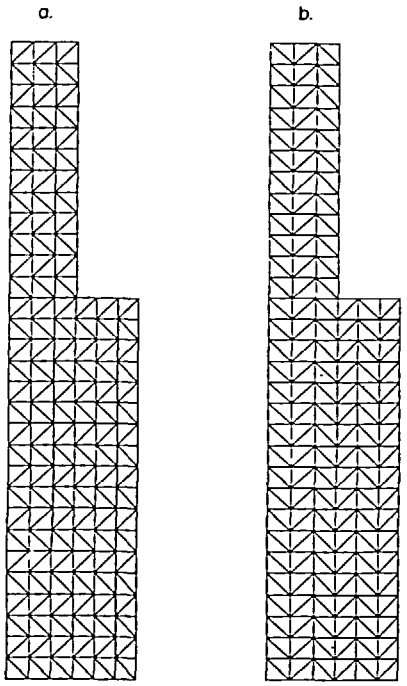

Figure 5 A portion of the computational grids: (a) the grid which resulted in the longest re-attachment lengths; (b) the grid which resulted in the shortest re-attachment lengths

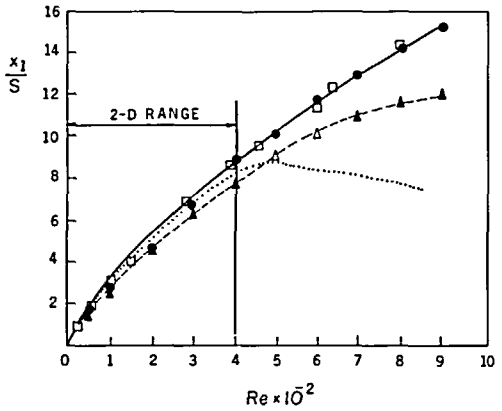

Figure 6 The re-attachment length: □, experimental results of Armaly *et al.*[3] for the centreline of the experimental setup; · · · · ·, numerical results of Armaly *et al.*[3]; –●–, results derived using the grid of *Figure 5a*; –▲–, results derived using the grid of *Figure 5b*; –△–, two points which required temporal relaxation

grid which was refined only in the stream-wise direction. The elements aspect ratio was thus varied from 1:1 to 3:1. These variations in the elements aspect ratio had no observable effect on the convergence rate of the scheme and the results were quite similar to those which are presented. In a driven cavity calculation, an aspect ratio of 30:1 was accidentally used and the solutions converged to physically reasonable results. This tolerance for variations in the elemental geometries again indicates the importance of accurate, analytically derived criteria for the required amount of artificial viscosity.

The results shown in *Figure 4* were computed using the grid of *Figure 5a*. *Figure 6* compares the previously shown results which were computed using the grid of *Figure 5a* (circles) with the results computed using the grid of *Figure 5b* (triangles). For both cases the artificial viscosity given by (34) was used. There is a significant discrepancy between the two sets of results but only at and above a Reynolds number of 400. This discrepancy is an indication of the error emanating from the use of a coarse grid. Such a discrepancy does not appear when the above grids are refined. This is in agreement with the common wisdom that the mesh spacing should be smaller by an order of magnitude than the typical dimensions of the physical problem. For the backward facing step problem, the next section introduces a mesh whose spacing is smaller by an order of magnitude than the step height, which is equal to the width of the recirculating zone.

As was already noted, the main objective of the present work was to achieve a non-oscillatory behaviour of the converged results of the iterative solution process. A byproduct of this suppression of spurious oscillations is that the convergence process itself is very robust. In the

present work, the equations were solved using a full Newton–Raphson linearization of all of the equations (save the term whose absolute value was raised to the d power). This linearization showed a large radius of convergence thus indicating that excessive spurious oscillations did not appear in the intermediate results of the iterative producer: Only two points required a temporal relaxation although a very crude initial guess of the velocity distribution was intentionally used for the other points (a parabolic velocity profile was imposed everywhere, including the points immediately upstream and immediately downstream of the step). For these two points the fluid was initially at rest and the boundary conditions were imposed in one time step. The time step was chosen so as to make the maximal Courant number in the flow field equal to 89. Therefore only a few time steps were required to reach the steady state. Convergence of the solution could not be achieved with longer time steps (i.e. with a higher Courant number).

The two points which required temporal relaxation are marked in *Figure 6* with open triangles. They fall in line with the other points thus indicating that the present scheme is conservative despite the use of the seven point integration scheme of Hammer *et al.*[7] without an integration by parts of the convective fluxes. This point was also verified by calculating a few points using an inefficient but accurate integration scheme which was fabricated using one-dimensional Gauss–Legendre and Gauss–Jacobi integrations as in Reference 7.

FINAL RESULTS

Armaly *et al.*[3] showed an additional recirculation zone which first appears at a critical Reynolds number of 400. *Figure 7a* shows this zone and defines its characteristic lengths x_2 and x_3. The cross-stream dimension of this zone is too small to be discerned when the previous coarse grid is used. To make a more complete simulation of the flow field the mesh spacings in both the x and y dimensions were halved. This quadrupled the number of the equations and doubled the bandwidth of the resulting matrix and consequently the radius of convergence of the scheme deteriorated so much that even temporal relaxation was not helpful. A more accurate initial estimate of the velocity distribution had to be used and therefore the velocity distribution which was calculated at a Reynolds number of 550 was used as an initial estimate for the higher Reynolds numbers.

Figure 7 depicts the results of the calculations which used the refined grid. Here, the refinements of both of the grids of *Figure 5* gave practically identical results and so did the different viscosity coefficients of the previous analysis. In *Figure 7* the numerical results of Armaly *et al.*[3] are again shown with dotted lines, their experimental results with squares and the present results with solid lines connecting shadowed circles. *Figure 7* clearly shows that the present results are far more accurate than the numerical results which Armaly *et al.*[3] calculated using TEACH. The present results regarding x_1 are identical to the experimental results of Armaly *et al.* up to a Reynolds number of 400, where the latter are two dimensional. This was already shown in *Figure 4* and therefore the present results (solid lines) begin at a Reynolds number of 500. At higher Reynolds numbers the results converge, as they should, to the average re-attachment length of the experiments rather than to the results which Armaly *et al.*[3] measured at the centreline of their experimental setup. This is shown by the starred point at a Reynolds number of 648 (Armaly *et al.*[3] very thoroughly documented the three-dimensional effects which occurred in the Reynolds number range of 400 to 6600. However, they published the data necessary for the calculation of the average re-attachment length only for two points and only this one is within the range of the present calculations). The results of Armaly *et al.*[3] for x_2 and x_3 which appear in *Figure 7b* are qualitatively wrong and they worsen as the Reynolds number increases. The present results are in a fairly good agreement with the experimental results for x_2 and they very closely resemble the experimental results for x_3 up to a Reynolds number of 1200 where the flow becomes turbulent. Kaiktsis *et al.*[8] compared their results for x_1 to those of others up to a Reynolds number of 800. These results agree with those of *Figure 7* and they took 30 min to

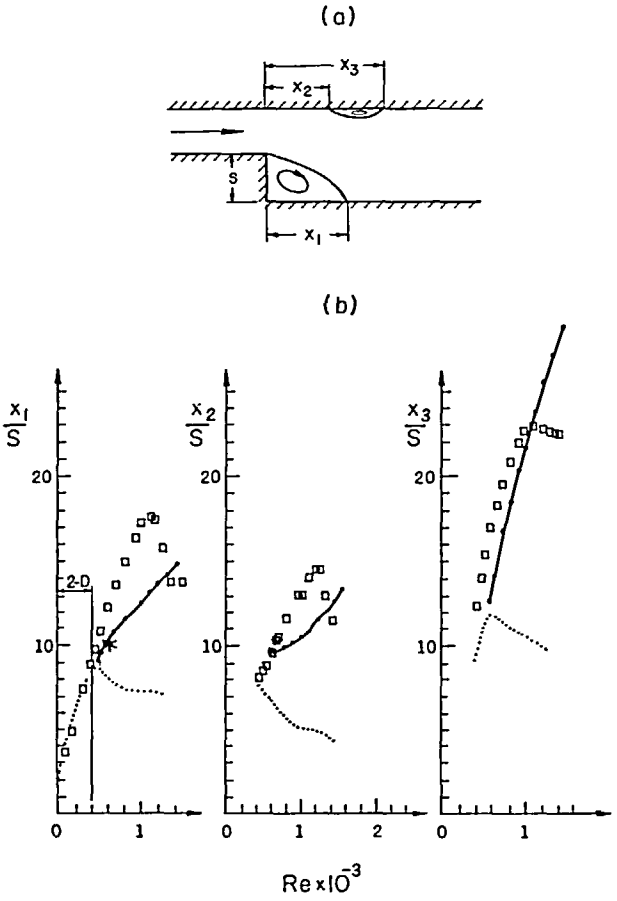

Figure 7 The detachment and re-attachment lengths: (a) a definition of the re-attachment lengths; (b) the experimental and numerical results: □, experimental results of Armaly *et al.*[3] for the centreline of the experimental setup; *, average of the experimental results of Armaly *et al.*[3] for Re = 648; ·····, numerical results of Armaly *et al.*[3]; –●–, results derived using a refinement of the grid of *Figure 4a*

compute on a Cray-Y/MP1. The present scheme allows us to improve efficiency by lowering the resolution of the numerical grid and therefore a typical run required less than 9 min on a DECstation 5000/240.

In the calculation of turbulent flows, the turbulent viscosity usually makes v large enough to prevent the appearance of spurious oscillations and to accordingly make v_a equal to zero [through (27)]. Since v_a is the subject of the present work, a turbulence model was not incorporated into the present program and the results for a Reynolds number above 1200, where turbulence begins, are presented only for completeness.

For additional verification of the present scheme, it was also used to simulate the flow in a driven cavity. The results for a Reynolds number of 5000 are shown and compared to the numerical results of Ghia *et al.*[2] in *Figure 8*. *Figure 8a* is a vector plot of the flow in the driven cavity and the boundary conditions are shown on it. *Figure 8b* shows the horizontal velocity profile in the centreline of the cavity. The squares show the results of Ghia *et al.*[2] wherein the grid divided the cavity into 256 × 256 squares. The line in *Figure 8b* shows the present results wherein the grid divided the cavity into 20 × 20 rectangles, each of which was subdivided into

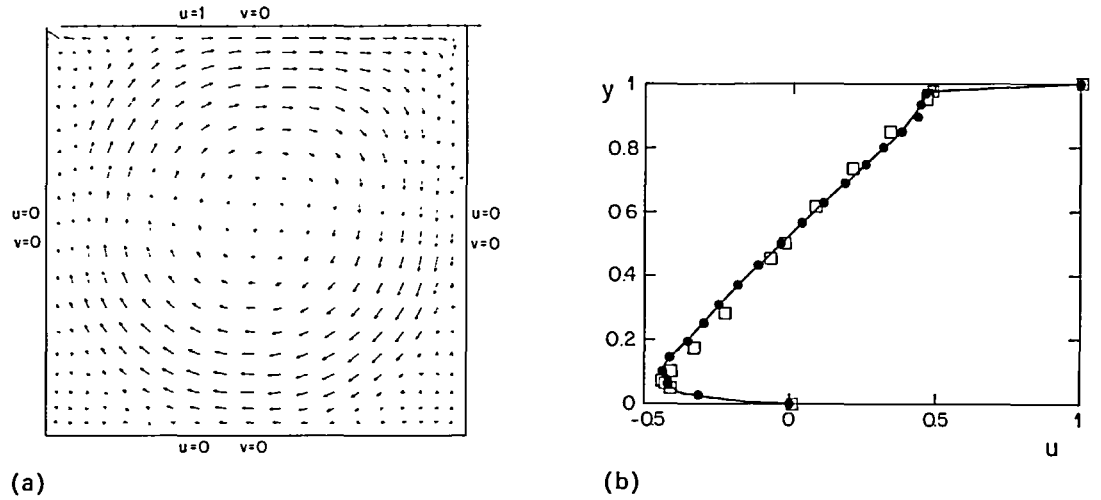

Figure 8 The driven cavity for $Re = 5000$: (a) vector plot; (b) the horizontal velocity at the centreline; –●–, marks the present results using a 20×20 grid; □, numerical results of Ghia *et al.*[2] who used a 256×256 grid

two triangular elements. The close agreement of the present results with the results of Ghia *et al.* is indeed an appropriate demonstration of the effectiveness of the proposed scheme.

Ghia *et al.*[2] used Rubin and Khosla's deferred correction upwinding procedure, which is an artificial dissipation scheme whose converged solutions are of a second-order accuracy, at the end of a temporal discretization. The present scheme is also of a second order accuracy but it does not require the use of a temporal relaxation.

CONCLUSIONS AND DISCUSSION

A robust and reasonably accurate artificial dissipation scheme for the Navier–Stokes equations was presented. The scheme consists of adding an artificial dissipation term to the equations along with a correction term which cancels the artificial term in the limit when the mesh size is zero. This ensures that with grid refinement the results of the scheme converge to a value which is independent of the artificial terms. Equation (7) illustrates that the correction term is a coarser discretization of the artificial term. The addition of such a term may perhaps be possible with other discretization methods and with other kinds of artificial terms. For the present application and for a finite mesh size, the correction term replaces the artificial viscosity terms with hyperviscosity terms, i.e., with an artificial dissipation which depends on the fourth derivatives of the velocity. Hyperviscosity more effectively suppresses the higher wave number modes and has a smaller effect on the inertial modes of the flow field than does artificial viscosity.

Also presented was a criterion for the required amount of artificial dissipation which correctly takes into account the flow velocity as well as the elemental geometry. The criterion was derived by considering the discretization of a model equation about the internal node of a triangular element. This process may perhaps be replicated for other elements and other schemes. The criterion was then empirically refined to suit the present scheme for the Navier–Stokes equations. Finally, the scheme was used to calculate the flow in a driven cavity and over a backward facing step. Due to the careful use of the artificial dissipation, the results are accurate even when a coarse grid is used.

ACKNOWLEDGEMENTS

We are grateful for very helpful discussions with Dr Yoram Yadlin of Fluent Inc. and Dr Yehuda Tassa of the Lockheed Missile and Space Corp. of Palo Alto, CA. One of the authors (A.K.) acknowledges much encouragement and support by Prof. Ozer Igra of Ben Gurion University of the Negev.

REFERENCES

1 Patankar, S. *Numerical Heat Transfer and Fluid Flow*, Hemisphere, New York, p. 37 (1980)
2 Ghia, U., Ghia, K. N. and Shin, C. T. High-Re solutions for incompressible flow using the Navier–Stokes equation and a multigrid method, *J. Comput. Phys.*, **48**, 387 (1982)
3 Armaly, B. F., Durst, F., Pereira, J. C. F. and Schönung, B. Experimentation and theoretical investigation of backward-facing step flow, *J. Fluid Mech.*, **127**, 473 (1983)
4 Thomas, C. E., Morgan, K. and Taylor, C. A finite element analysis of flow over a backward facing step, *Comp. Fluids*, **9**, 265 (1981)
5 Jiang, B. N. and Carey, G. F. Adaptive refinement for least-squares finite elements with element-by-element conjugate gradient solution, *Int. J. Num. Meth. Eng.*, **24**, 569 (1987)
6 Jiang, B. N. and Povinelli, L. A. Least-square finite element method for fluid dynamics, *Comp. Meth. Appl. Mech. Eng.*, **81**, 13 (1990)
7 Hammer, P. C., Marlowe, O. J. and Stroud, A. H. Numerical integration over simplexes and cones, *Math. Tables and Other Aids to Computation* (continued by *Math. Comput.*), **10**, 130 (1956))
8 Kaiktsis, L., Karmiadakis, G. E. and Orszag, S. A. Onset of three-dimensionality, equilibria, and early transition in flow over a backward-facing step, *J. Fluid Mech.*, **231**, 501 (1991)